

# ON THE TEMPERATURE AND INTENSITY DISTRIBUTION OF THE GALACTIC X-RAY PLASMA

M. Kappes, J. Pradas, and J. Kerp

Radioastronomisches Institut der Universität Bonn, Auf dem Hügel 71, 53121 Bonn, Germany

## ABSTRACT

We present the results of our investigation of the composition of the diffuse soft X-ray background emission (SXRb). Combining data of the Leiden/Dwingeloo HI Survey and the *ROSAT* All-Sky Survey (RASS), we set up a radiation transport equation in order to model the SXRb. Two different techniques lead to the model parameters: An image oriented approach which compares observed and modeled maps of the 1/4 and 3/4 keV X-ray energy regime and a more analytic approach using scatter diagrams.

The analysis shows that *only three* independent components of the emitting plasma (local, halo and extragalactic) are needed to explain the SXRb. The results for the temperatures and X-ray intensities, which characterize the three components, are given and compared to an alternative model.

Key words: Galaxy: halo – structure – ISM: HI – structure – X-rays

## 1. INTRODUCTION

To understand the origin and evolution of the Milky Way it is necessary to investigate its emission across the entire electromagnetic frequency spectrum. In the soft X-ray energy regime much progress was gained by the *ROSAT*-mission and its discovery of coronal gas located within the Milky Way halo (Snowden et al. 1991).

Today there is general agreement that we can identify at least three individual components which contribute to the diffuse soft X-ray background (SXRb) emission: The coronal gas partly filling the Local Bubble (Snowden et al. 1998), X-ray plasma localized within the Milky Way halo (Pietz et al. 1998) and finally the superposed emission of individual X-ray sources at extragalactic distances (Hasinger et al. 2001).

With *ROSAT*-all sky survey data it is possible to shed light on the physical properties of the several components of the SXRb. Questions we like to answer are: Is the halo plasma hotter or cooler than the local X-ray gas? Is there evidence for more than one single coronal gas phase in the Milky Way halo (Kuntz & Snowden 2000)? Is the plasma

emissivity a function of Galactic longitude and/or latitude (Pietz et al. 1998)?

## 2. DATA AND MODEL

The correlation of the *ROSAT* All-Sky Survey (RASS) 1/4 keV (*ROSAT*-C-band) and 3/4 keV (*ROSAT*-M-band) data with the Leiden/Dwingeloo HI Survey of galactic neutral hydrogen (Hartmann & Burton 1997) provides an opportunity to disentangle the different SXRb components. Figure 1 illustrates our approach to model the X-ray radiation transport through the Galactic interstellar medium. Because of the anti-correlation between X-ray radiation and HI column density it is possible to set up the following radiation transport equation:

$$I = I_l + I_h \cdot e^{-\sigma(E, N_{\text{HI},h}) \cdot N_{\text{HI},h}} + I_e \cdot e^{-\sigma(E, N_{\text{HI},e}) \cdot N_{\text{HI},e}} \quad (1)$$

$I_l$  denotes the Local Bubble component,  $I_h$  denotes the halo component and  $I_e$  the extragalactic contribution. The observed X-ray intensity distribution is modulated by photoelectric absorption traced by the HI gas. In our initial approach we include three X-ray emission components. First, an unabsorbed foreground Raymond-Smith plasma representing the Local Bubble emission, an absorbed distant Raymond-Smith plasma (halo component) and an absorbed extragalactic energy power-law (EPL) with index  $\alpha = -1.5$  (Hasinger et al. 2001).

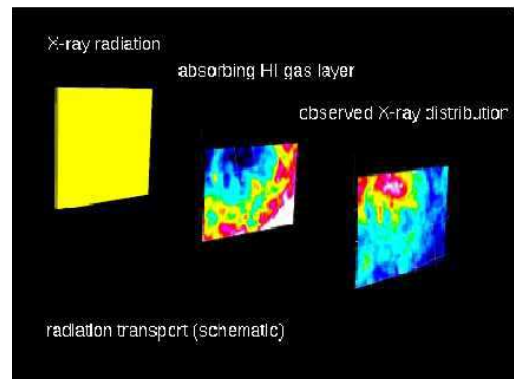


Figure 1. A homogeneous X-ray background is absorbed by the Galactic HI-layer and produces the observed X-ray distribution. This is just a simple illustration of the radiation transport approach according to Eq. 1

### 3. DERIVING THE MODEL PARAMETERS

We investigate two different fields: *Field A* at  $20^\circ < b < 47^\circ$ ,  $34^\circ < l < 85^\circ$  and *field B* at  $12^\circ < b < 74^\circ$ ,  $99^\circ < l < 166^\circ$ . These fields are at high Galactic latitude, where the smaller HI column density allows a better study of the halo component in comparison with the Galactic plane where this radiation is much stronger absorbed. Both fields cover a large range in HI column densities which improves the significance of the X-ray/HI correlation. Figure 3 shows the 1/4 keV *ROSAT*-band for *field A*.

#### 3.1. SCATTER DIAGRAMS

First, we evaluate the X-ray intensity of the Local Bubble. For this aim, we produce “scatter diagrams” which are shown in Fig. 2. At high column densities the distant and extragalactic X-ray components are so strongly absorbed that the remaining C-band intensity can be attributed entirely to the Local Bubble emission. We derive a Local Bubble intensity of  $I_l = 350 \cdot 10^{-6} \text{cts s}^{-1} \text{arcmin}^{-2}$  for both fields investigated.

Second, for the extragalactic background intensity we use the value  $I_e = (228 \pm 90) \cdot 10^{-6} \text{cts s}^{-1} \text{arcmin}^{-2}$  given by Barber et al. (1996), as a first estimate. The power-law index is fixed to  $\alpha = -1.5$  (Hasinger et al. 2001).

Third, we evaluate the contribution of the halo component to the SXR. Different values for the C-band intensity and temperatures of the Raymond-Smith plasma used, is combined with the corresponding theoretical band ratios.

It turns out that the C-band scatter diagram is *not* a sensible measure for halo plasma temperature; on the contrary the other energy bands and derived ratios are! Note especially the upper right diagram in Fig. 2: The curves for the three different temperatures are almost identical. Only in combination with the M-band scatter diagram and the C/M-band ratio it is possible to derive the temperatures reliably. Because of this finding, we have to fit *simultaneously* the R1-, R2-, C- and M-band data. The derived results – on temperature and intensity – are used to calculate model images (see Fig. 4) which we test independently as follows.

#### 3.2. MODELED IMAGES

By subtracting the modeled images from the observed ones (this is done pixel-by-pixel) we calculate absolute deviations between both which are divided by the uncertainty maps of the *ROSAT* observations in both C- and M-band. The resulting normalized deviation-distribution is a measure for the statistical significance of the model expressed in units of the standard deviation (e.g. if the deviation width is close to unity then the uncertainty of the model is comparable to the uncertainty of the *ROSAT* data).

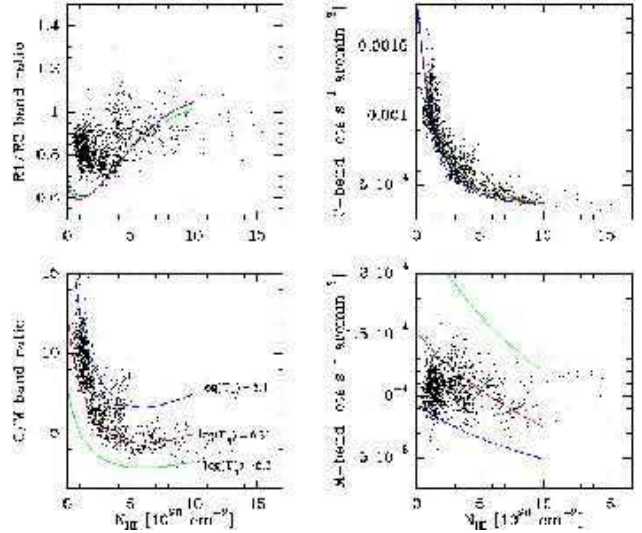


Figure 2. Scatter diagrams and energy band-ratios for **field B**. The three curves correspond to three different halo temperatures. Only the M-band and the C/M-band ratios are a good indicator to the different temperature estimates in contrast to the C-band. Note, that the C-band scatter diagram is not sensitive for different temperatures, i.e. the three curves are almost the same in the upper right diagram.

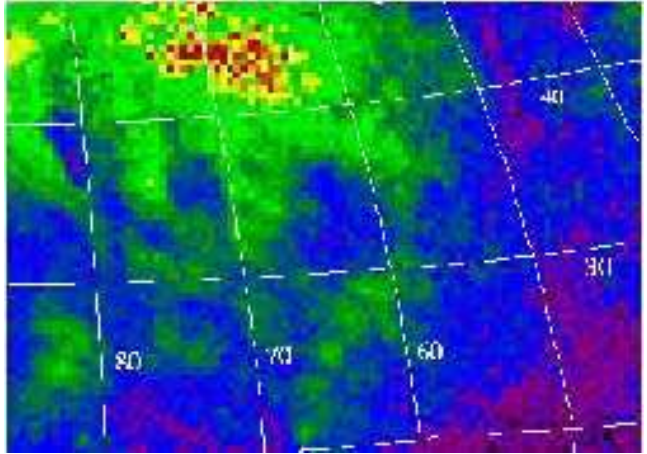


Figure 3. Observed X-ray intensity of **field A**, *ROSAT*-C-band.

We produce “deviation images” and superimpose their contour lines on the *ROSAT*-C-band model images, as shown in Fig. 4. At first glance it is clear that the deviations are not randomly distributed across the fields, but form coherent structures. The dotted contours correspond to areas where the modeled intensities are brighter than the observed ones, while the modeled intensity encircled by the solid contours is too faint. The regions with dotted contours can be explained by the lack of absorbing material, while the regions marked by solid lines represent excess emission or too much absorbing material. For ex-

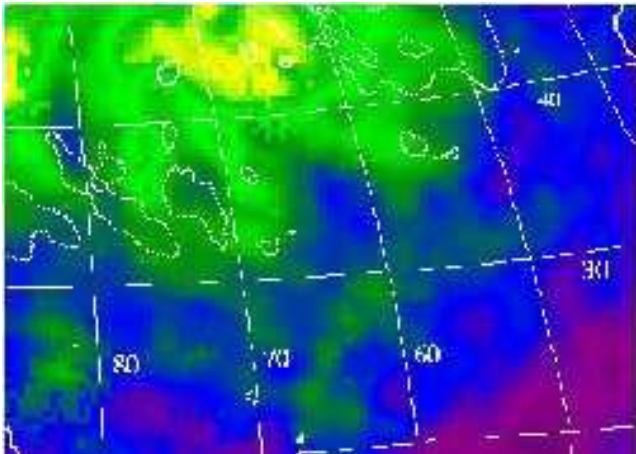


Figure 4. Modeled X-ray intensity of **field A**, ROSAT-C-band. The contours show areas for which the deviations between model and observation are greater than  $2.5\sigma$ .

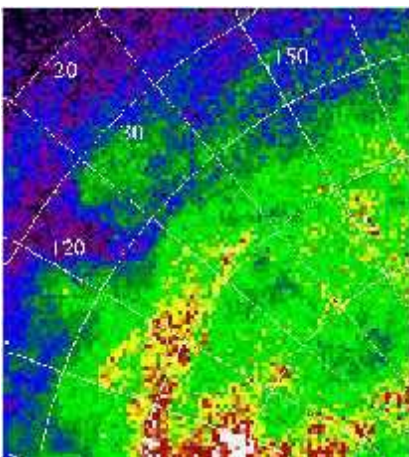


Figure 5. Observed X-ray intensity of **field B**, ROSAT-C-band.

ample, *field B* contains intergroup HI-gas belonging the M81 group of galaxies, which yields X-ray excess emission in the modeled intensity (see Fig. 6).

In order to minimize the misfitting regions, we subtract gas with velocities  $|v_{\text{LSR}}| \geq 25 \text{ km s}^{-1}$  from the HI data in the solid marked areas and it turns out that the model fits much better, without producing further excess emission. With this HI data selection, which is done for both fields, it is possible to reduce a huge area of excess emission in Fig. 4 to only three small spots. Unfortunately the dotted features cannot be identified.

#### 4. TESTING THE MODEL

To obtain better model parameters we take a closer look at the statistics of the deviations. Figure 7 illustrates the goodness of the model. The red plot represents the devia-

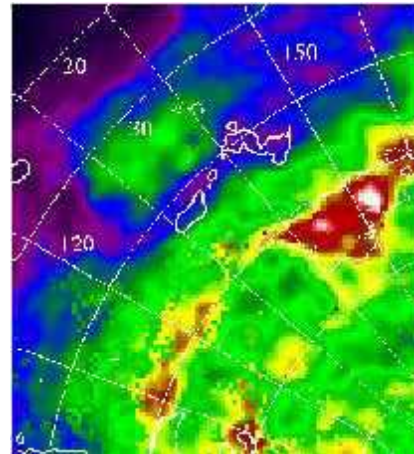


Figure 6. Modeled X-ray intensity of **field B**, ROSAT-C-band. The contours show areas for which the deviations between model and observation are greater than  $2.5\sigma$ . The dotted contours towards the Lockman-Area ( $(l, b) = (150^\circ, 53^\circ)$ ) indicate a lack of absorbing material, while the solid encircled area at  $(l, b) = (140^\circ, 40^\circ)$  corresponds to the M81 group of galaxies which increases the Galactic HI column density. Therefore the modeled X-ray intensity is too faint.

tion in the C-band while the blue plot corresponds to the M-band deviation.

The goal is to derive model parameters which lead to histograms with a mean  $\mu = 0$  and a standard deviation  $\sigma = 1$  simultaneously in both energy bands. This is done by an iterative process in which we vary the model parameters we initially obtained from the scatter diagrams and analyze the mean and standard deviation of their histograms. Varying  $I_e$ , it turns out, that a value of  $170 \cdot 10^{-6} \text{ cts s}^{-1} \text{ arcmin}^{-2}$  fits much better than the original value given by Barber et al. (1996). In addition to our model we fit another model with two distant halo components as proposed by Kuntz & Snowden (2000). For the statistical significance see Fig. 8. Note, that both energy bands are independent from each other in the two distant halo component model, i.e. they cannot be fitted simultaneously, in contrast to our approach.

The best fitting model intensities are shown in Tab. 1 for the observed fields. The best fitting temperature for the Local Bubble is  $\log(T_1)=5.9$  and for the Halo we derive  $\log(T_h)=6.2$ . For the two halo component model we adopt the temperatures derived by Kuntz & Snowden (2000):  $\log(T_1)=6.1$ ,  $\log(T_{h_1})=6.0$ , and  $\log(T_{h_2})=6.4$ .

The intensities found for *field A* and *B* differ by about 40% which can be attributed to a variation in intensities with Galactic latitude and/or longitude (see Tab. 1). This behavior is *not* expected with the two distant component model proposed by Kuntz & Snowden (2000). A more detailed study of the  $l, b$ -dependency will be presented in a forthcoming paper.

Field A	$I_l$	$I_h$	$I_e$
1/4 keV	350	1975	170
3/4 keV	1	152	40
Field B			
1/4 keV	350	1380	170
3/4 keV	1	110	40
Field A			
1/4 keV	350	1380,1100	230
3/4 keV	12	15,282	53

Table 1. The upper two sections compile the best fitting intensities for the fields A and B. The third section contains the values for field A according to the two halo component model by Kuntz & Snowden (2000). All intensities are in units of  $10^{-6}$ cts  $s^{-1}$  arcmin $^{-2}$ .

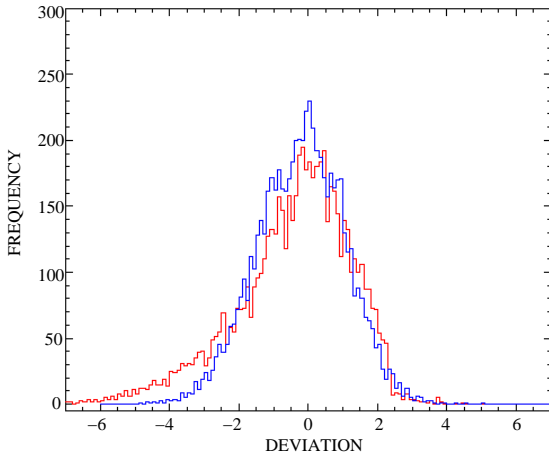


Figure 7. This histogram refers to field A where the red curve is the deviation of the C-band and the blue curve corresponds to the M-band.

## 5. SUMMARY

- The Local Bubble appears as a one component X-ray plasma with a temperature of  $T = 10^{5.9}$  K and an intensity of  $350 \cdot 10^{-6}$ cts  $s^{-1}$  arcmin $^{-2}$  in the 1/4-keV energy regime. Moreover, the contribution of the halo exceeds the local distribution by a factor of four.
- The remaining SXRb is compatible with the following: A one component halo plasma with a temperature of  $T = 10^{6.2}$  K and varying intensity in both latitude and longitude. Note, that it is not necessary to introduce *more* than one halo component. Furthermore, an extragalactic component with an intensity of  $170 \cdot 10^{-6}$ cts  $s^{-1}$  arcmin $^{-2}$  is found, which is consistent with the value provided by Barber et al. (1996)
- The variation with Galactic latitude and longitude suggests the existence of a smoothly distributed halo plasma which surrounds the Milky Way.

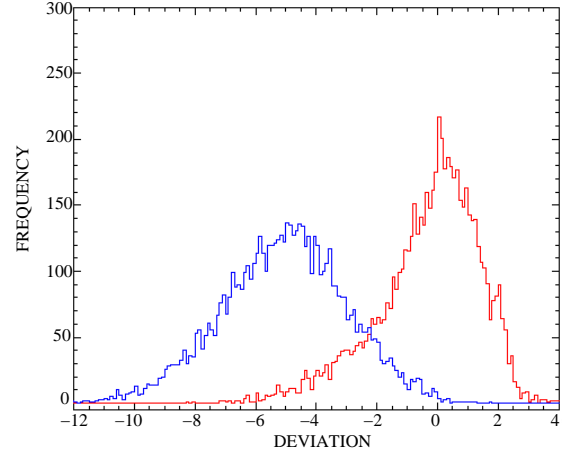


Figure 8. Statistical significance for the two distant-component model by Kuntz & Snowden (2000) for field A. The red curve is the deviation of the C-band and the blue curve corresponds to the M-band.

## ACKNOWLEDGEMENTS

The authors like to thank the Deutsches Zentrum für Luft- und Raumfahrt for financial support under grant No. 50 OR 0103.

## REFERENCES

- Barber, C. R., Roberts, T. P., Warwick, R. S. 1996, MNRAS 282, 157B
- Hartmann, D., Burton, W. B. 1997, Atlas of galactic neutral hydrogen, Cambridge University Press
- Hasinger, G., Altieri, B., Arnaud, M., Barcons, X., Bergeron, J., Brunner, H., Dadina, M., Dennerl, K., Ferrando, P., Finoguenov, A., Griffiths, R. E., Hashimoto, Y., Jansen, F. A., Lumb, D. H., Mason, K. O., Mateos, S., McMahon, R. G., Miyajiri, T., Paerels, F., Page, M. J., Ptak, A. F., Sasseen, T. P., Schartel, N., Szokoly, G. P., Trümper, J., Turner, M., Warwick, R. S., Watson, M. G. 2001, A&A 365L, 45H
- Kuntz, K. D., Snowden, S. L. 2000, ApJ 543, 195K
- Pietz, J., Kerp, J., Kalberla, P. M. W., Burton, W. B., Hartmann, Dap, Mebold, U. 1998, A&A 332, 55P
- Snowden, S. L., Egger, R., Finkbeiner, D. P., Freyberg, M. J., Plucinsky, P. P. 1998, ApJ 493, 715S
- Snowden, S. L., Plucinsky, P. P., McCammon, D., Freyberg, M. J., Schmitt, J. H. M. M., Trümper, J. 1991, BAAS 23, 1400S